IET Control Theory & Applications

*Research Article*

IET Journals
The Institution of Engineering and Technology

ISSN 1751-8644
doi: 0000000000
www.ietdl.org

# Hierarchical Global Fast Terminal Sliding Mode Control for A Bridge Traveling Crane System

*Weilin Yang*[1] *Jiayu Chen*[1] *Dezhi Xu*[1] ✉ *Xinggang Yan*[2]

[1] *School of Internet of Things Engineering, Jiangnan University, Wuxi, 214122, China*
[2] *School of Engineering and Digital Arts, University of Kent, Canterbury, CT2 7NT, UK*
** E-mail: lutxdz@126.com, xudezhi@jiangnan.edu.cn*

**Abstract:** The bridge crane system is a typical under-actuated system that is widely used in production and life. Although various scholars have conducted extensive research on the bridge crane system in recent years, there are still many problems, such as the trajectory planning of the cart and the anti-sway control of the payload.In order to tackle the problem of the anti-sway control of the payload, a hierarchical global fast terminal sliding mode control(H-GFTSMC) is developed in this paper. First, the Lagrange equations are used to model the system dynamics. Then, appropriate hierarchical global fast terminal sliding mode controller is designed to achieve anti-sway control of the payload and it is proven that each sliding mode surface is progressively stable. A series of simulations were implemented to verify the effectiveness of the control method. The simulation results show that the control method has better control performance than the traditional PID control method. At the same time, when changing the cable length or adding non-negligible noise to the system, the control method still has good robustness.

## 1 Introduction

The bridge crane system is widely used as an important loading equipment various industries, such as port transportation, and equipment manufacturing[1, 2]. During the transportation of the bridge crane system, the inertia caused by the acceleration and the deceleration of the cart and the trolly and the lifting action will cause the payload to swing back and forth. This not only increases the possibility of accidents, but also seriously affects the improvement of production efficiency. Currently, the solution to this problem rely on the actual operating experience of the operator, which can realize the safe transportation and unloading of the payload [3–6]. However, due to the long training period of the skilled technicians and the excessive work intensity, the working efficiency of the overall bridge traveling crane system is significantly restricted. Therefore, there is an urgent need for the automatic control system of the bridge crane system to solve the excessive dependence on operator experience [7–9]. The control of the bridge crane system includes many aspects, such as the positioning of the cart, the trajectory planning of the cart and the anti-sway control of the payload [10, 11]. The anti-sway control of the payload is the core problem of the automatic control of the bridge crane system [12, 13]. Numerous methods, including the PID control method have been proposed by scholars [14].

In recent years, numerous studies have been conducted on this issue. The traditional PID control method is relatively simple to implement and is currently the most widely used control method in practice. In [15–18], some improvements to traditional PID have been proposed. In [15, 16] Soukkou A and Ko C N combined the fuzzy control with the PID control and designed a Fuzzy-PID controller. Piccagli, S proposed a PID controller for Lagrange system in [17]. Recently, Cuoghi[18] proposed a new formulae for the design of the PID controller for better steady-state performance and robustness. In [19], Ahmad M A proposed a single input fuzzy control for a double-pendulum-type overhead crane. In [20], Konstantopoulos proposed an open-loop and a closed-loop control scheme and combined them together. Some scholars have applied a variety of intelligent control methods to control the bridge crane systems. J. A. Mendez [21] designed a neural network based self-tuning controller for an overhead crane. In [22], Zhu X presented a novel radial basis function neural network modeling method. In [23, 24], Petrenko Y N and Jahedi G combined the idea of genetic algorithm and fuzzy control and achieved good results. Many scholars used the sliding mode control method to conduct the research. The sliding mode control offers a good capability to achieve high tracking performance and preserve strong robustness. Wang W presented two sliding-mode controller models for a class of under-actuated systems[25]. Liu D [26] designed an adaptive sliding mode fuzzy control approach. Sun[27] constructed a sliding-mode-like strategy as well as an integral manifold. In [28], Tuan L A proposed a second-order sliding mode controller for a three-dimensional overhead crane in an extremely complicated operation with uncertain system parameters. Morever, for uncertain systems, Xi Z [29] proposed an integral sliding mode control method for discrete time systems. In [30], Lin F designed a robust fuzzy neural network (RFNN) sliding-mode control for a two-axis motion control system.

The sliding mode control has a good control performance in the control of general nonlinear systems. However, the traditional sliding mode method will have certain disadvantages for under-actuated systems, such as difficulty in eliminating the sliding surface chattering, or slow system response speed. Considering that the bridge crane system hsa a characteristic of being under-actuated, this paper proposes a H-GFTSMC referring to [31]. The main contributions of this paper are as follows:

(i) A controller is designed and compared with the traditional methods. Moreover, the inherent error or the interference in the system is observed and compensated in the controller.
(ii) Considering the performance of cable length on robustness, the proposed controller can adapt to a larger range of cable lengths and maintain robustness.
(iii) Considering the influence of noise on the robustness of the system, the controller can still maintain good robustness under the condition of a certain range of noise.

The next section models the bridge crane system. In section III, a hierarchical global fast terminal sliding mode controller is established that is suitable for the bridge crane system. In section IV, the stability of the proposed controller is validated. A series of simulation results is presented in section V. Section VI contains the final conclusions.

## 2 Modeling of a bridge crane system

### *2.1 The main structure and characteristics of the bridge crane system*

There are three driving devices for bridge cranes, including a cart operation mechanism, a trolley operation mechanism and a lifting mechanism. The cart runs along the tracks laid on both elevated sides. The track laid on the bridge runs in order to ensure that the payload can be carried in the three-dimensional space. Among them, the cart operating mechanism is responsible for moving the whole machine along the tracks laid on the two sides of the overhead, the trolley is responsible for the movement of the suspended object on the bridge, and the lifting mechanism is responsible for the vertical movement of the suspended object. While the operation of bridge crane, these three mechanisms may operate at the same time or in different combinations.

In the bridge crane system, if only a cart or a trolly is in operation, the crane will move in a two-dimensional plane, with the following two degrees of freedom: the displacement of the cart and the swing angle of the lifting payload, as shown in Fig.1(a). If the lifting mechanism also runs with the cart or the trolly, the bridge crane will have three degrees of freedom, as shown in Fig.1(b). When both the cart and the trolly are running at the same time, the bridge crane and the lifting payload will move in a three-dimensional space, as shown in Fig.1(c). If the lifting mechanism is operated together with the cart and the trolley, the bridge crane system will have five degrees of freedom, as shown in Fig.1(d).

In order to facilitate the modeling and simulation of the proposed controller, following assumptions are made:

(i) The spreaders and the payload are treated as a particle.
(ii) Air resistance and wind effects are ignored.
(iii) The quality and the elasticity of the cable are ignored.
(iv) The friction at the connection between the wire cable and the trolley is ignored.
(v) The non-linearitise of the transmission mechanism such as the trolley motor and the reducer are ignored. It is believed that the driving force of the trolley can be directly controlled by the output torque of the controller.

### *2.2 Dynamics modeling*

It is difficult to modeling a crane system because it is an unstable under-actuated system. So the Lagrange equation is used to mathematically model the dynamic model of the bridge crane system.

The general form of the Lagrange equation:

$$\frac{d}{dt}(\frac{\partial L}{\partial \dot{q}_i}) - \frac{\partial L}{\partial q_i} = Q_i (i = 1, 2, 3, 4, 5) \tag{1}$$

where $q_i$ is generalized coordinates, $K = \sum_{t=1}^{n} \frac{1}{2} m_t v_t^2$ is Lagrangian kinetic energy of particle system, $P$ is potential energy of particles, $L = K - P$ is lagrange function, $Q_i$ is generalized force of particle system.

Considering that the main part of the dissipative force in the system is friction, which cannot be ignored. So a dissipative force term is added to the general form of the Lagrange equation[32]. Then the Lagrange equation with dissipative force term can be got.

$$\frac{d}{dt}(\frac{\partial L}{\partial \dot{q}_i}) - \frac{\partial L}{\partial q_i} + \frac{\partial F}{\partial \dot{q}_i} = Q_i (i = 1, 2, 3, 4, 5) \tag{2}$$

where $F$ is dissipative force function.

A 3D, 4-dof model is been selected as the research object, as is shown in Fig.1(c), where $M$ is total mass of the cart and trolly, $m$ is the mass of the payload and its rotating system, $l$ is the cable length, $XYZ$ coordinate system is a fixed coordinate system with the initial position of the trolly as the origin, $X_M Y_M Z_M$ is a coordinate system with the cart's current position as the origin. The coordinate of the trolley on the $XYZ$ coordinate system is $(x, y, 0)$, at the same time each axis of the trolley coordinate system is parallel to the corresponding axis of the fixed coordinate system. And $Y_M$ is defined along the main beam, the direction of movement of the trolley is $Y_M$, the direction of movement of the main beam is $X_M$. $\theta$ is the angle between the hoisting payload in any direction and the vertical direction. This angle has two components that can be decomposed into $\theta_x$ and $\theta_y$. $\theta_x$ is the component of $\theta$ on the $X_M O Z_M$ plane, $\theta_y$ is the component of $\theta$ on the $Y_M O Z_M$ plane.

If it is assumed that the coordinate of the lifting payload in the $XYZ$ coordinate system is ($x_m$,$y_m$,$z_m$), which is given by

$$\begin{aligned} x_m &= x + l \sin\theta_x \cos\theta_y, \\ y_m &= y + l \sin\theta_y, \\ z_m &= -l \cos\theta_x \cos\theta_y. \end{aligned} \tag{3}$$

where $l$ is the cable length.

The kinetic energy of the crane and its payload, the potential energy of the payload and dissipative force function are given as

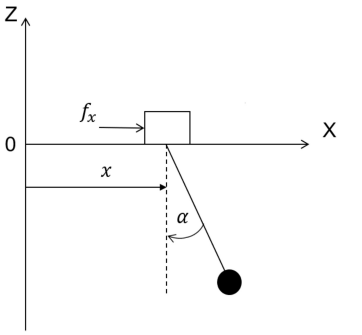

(a)

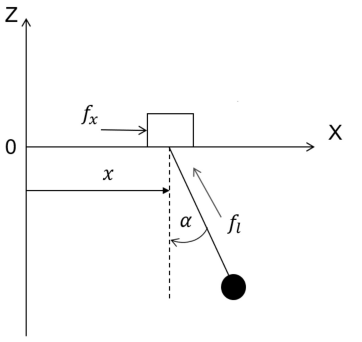

(b)

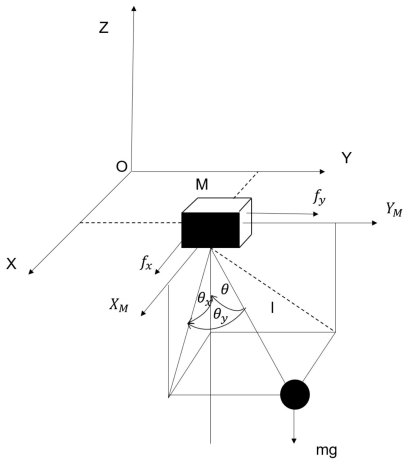

(c)

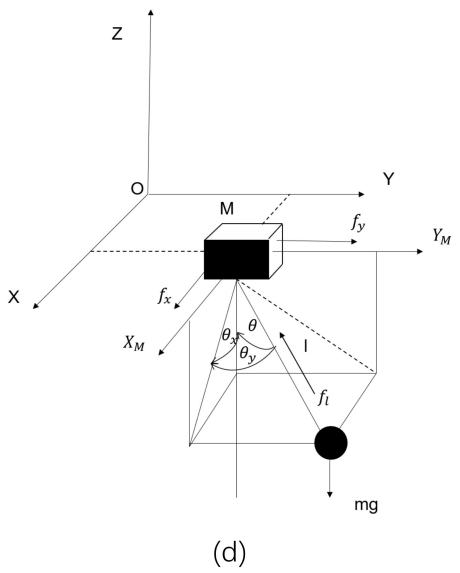


**Fig. 1:** Bridge crane system model: 2D, 2-dof(a), 2D, 3-dof(b), 3D, 4-dof(c), 3D, 5-dof(d)

follows

$$\begin{aligned} K &= \frac{1}{2}(M_x\dot{x}^2 + M_y\dot{y}^2 + M_l\dot{l}^2) + \frac{m}{2}v_m^2, \\ P &= mgl(1-\cos\theta_x\cos\theta_y), \\ F &= \frac{1}{2}(D_x\dot{x}^2 + D_y\dot{y}^2 + D_l\dot{l}^2). \end{aligned} \tag{4}$$

where $v_m^2$ is given as follows

$$\begin{aligned} v_m^2 &= \dot{x}_m^2 + \dot{y}_m^2 + \dot{z}_m^2 \\ &= \dot{x}^2 + \dot{y}^2 + l^2\cos^2\theta_y\dot{\theta}_x^2 + l^2\dot{\theta}_y + 2l\cos\theta_y\dot{\theta}_y\dot{y}. \\ &\quad + 2(l\cos\theta_x\cos\theta_y\dot{\theta}_x - l\sin\theta_x\sin\theta_y\dot{\theta}_y)\dot{x}. \end{aligned} \tag{5}$$

The Lagrangian $L$ is defined as $L = K - P$.

For the 4-dof bridge crane system model shown in Fig.1(c), that is to say the cable length will not change during the movement, so $\dot{l} = \ddot{l} = 0$, substituting it into Eqn.(3) and Eqn.(4) gives the Lagrange function $L$ and dissipative Force Function $F$ as follows

$$\begin{aligned} L =& K - P \\ =& \frac{1}{2}(M_x\dot{x}^2 + M_y\dot{y}^2) + \frac{m}{2}v_m^2 \\ & - mgl(1-\cos\theta_x\cos\theta_y), \\ F =& \frac{1}{2}(D_x\dot{x}^2 + D_y\dot{y}^2). \end{aligned} \tag{6}$$

where $v_m^2$ is given as follows

$$\begin{aligned} v_m^2 &= \dot{x}_m^2 + \dot{y}_m^2 + \dot{z}_m^2 \\ &= \dot{x}^2 + \dot{y}^2 + l^2\cos^2\theta_y\dot{\theta}_x^2 + l^2\dot{\theta}_y + 2l\cos\theta_y\dot{\theta}_y\dot{y} \\ &\quad + 2(l\cos\theta_x\cos\theta_y\dot{\theta}_x - l\sin\theta_x\sin\theta_y\dot{\theta}_y)\dot{x}. \end{aligned} \tag{7}$$

where $M_X$ and $M_Y$ are the $x$(traveling) and $y$(traversing) components of the crane mass and the equivalent masses of the rotating parts such as the motors and their drive trains; the quantities $m$, $g$ and $v_m$ denote the payload mass, the gravitational acceleration, and the payload speed, respectively.

The equations of motion of the crane system are obtained by substituting $L$ and $F$ into Lagrange's equations associated with the generalized coordinates $x$, $\theta_x$, $y$, $\theta_y$ and $l$. After some manipulations, the following four second-order ordinary differential equations are obtained

$$\begin{aligned} &(M_x+m)\ddot{x} + ml\cos\theta_x\cos\theta_y\ddot{\theta}_x - ml\sin\theta_x\sin\theta_y\ddot{\theta}_y \\ &+ D_x x - ml\sin\theta_x\cos\theta_y\dot{\theta}_x^2 - 2ml\cos\theta_x\sin\theta_y\dot{\theta}_x\dot{\theta}_y \\ &- ml\sin\theta_x\cos\theta_y\dot{\theta}_y^2 = f_x, \end{aligned} \tag{8}$$

$$(M_y+m)\ddot{y} + D_y\dot{y} + ml\cos\theta_y\ddot{\theta}_y - ml\sin\theta_y\dot{\theta}_y^2 = f_y, \tag{9}$$

$$\begin{aligned} &ml^2\cos^2\theta_y\ddot{\theta}_x + ml\cos\theta_x\cos\theta_y\ddot{x} + mgl\sin\theta_x\cos\theta_y \\ &- 2ml^2\sin\theta_y\cos\theta_y\dot{\theta}_x\dot{\theta}_y = 0, \end{aligned} \tag{10}$$

$$\begin{aligned} &ml\cos\theta_y\ddot{y} - ml\sin\theta_x\sin\theta_y\ddot{x} + ml^2\cos\theta_y\sin\theta_y\dot{\theta}_x^2 \\ &+ mgl\cos\theta_x\sin\theta_y + ml^2\ddot{\theta}_y = 0. \end{aligned} \tag{11}$$

where $f_x$ and $f_y$ are the driving forces of the motions in the X-direction and the Y-direction.

The dynamic model of the 3D crane system in Eqn.(8)-(11) can be represented using the compact form

$$M(q)\ddot{q} + D\dot{q} + C(q,\dot{q})\dot{q} + G(q) = F. \tag{12}$$

where

$$q = \begin{bmatrix} x & y & \theta_x & \theta_y \end{bmatrix}^T, \tag{13}$$

$$M(q) = \begin{bmatrix} M_{11} & M_{12} & M_{13} & M_{14} \\ M_{12} & M_{22} & M_{23} & M_{24} \\ M_{13} & M_{32} & M_{33} & M_{34} \\ M_{14} & M_{42} & M_{43} & M_{44} \end{bmatrix}, \tag{14}$$

$$C(q,\dot{q})\dot{q} = \begin{bmatrix} 0 & 0 & C_{13} & C_{14} \\ 0 & 0 & C_{23} & C_{24} \\ 0 & 0 & C_{33} & C_{34} \\ 0 & 0 & C_{43} & C_{44} \end{bmatrix}, \tag{15}$$

$$D = \begin{bmatrix} D_x & 0 & 0 & 0 \\ 0 & D_y & 0 & 0 \\ 0 & 0 & 0 & 0 \\ 0 & 0 & 0 & 0 \end{bmatrix}, \tag{16}$$

$$G(q) = \begin{bmatrix} 0 \\ 0 \\ mgl\sin\theta_x\cos\theta_y \\ mgl\cos\theta_x\sin\theta_y \end{bmatrix}. \tag{17}$$

please refer to the Appendix 1 for details.

Combining $C(q,\dot{q})$ and $D$ into $\bar{C}(q,\dot{q})$, then Eqn.(12) is simplified as follows

$$M(q)\ddot{q} + \bar{C}(q,\dot{q})\dot{q} + G(q) = F. \tag{18}$$

where

$$\bar{C}(q,\dot{q})\dot{q} = \begin{bmatrix} D_x & 0 & C_{13} & C_{14} \\ 0 & D_y & C_{23} & C_{24} \\ 0 & 0 & C_{33} & C_{34} \\ 0 & 0 & C_{43} & C_{44} \end{bmatrix}. \tag{19}$$

## 3 Design of hierarchical global fast terminal sliding mode controller

The crane model given in Eqn.(8)-(11) represents the model of an under-actuated system. Generally speaking, the control of under-actuated systems is inconvenient. Therefore, a H-GFTSMC method

is used to solve this problem. For under-actuated systems, the basic idea of the H-GFTSMC method is to divide the actuated and the under-actuated parts of the system into different sub-systems, design the lower layer sub-sliding surfaces, and then construct the total sliding surface of the upper layer system from the sub-sliding surfaces as is shown in Fig.2. The global fast terminal sliding mode is selected as the sub-sliding mode surface. The global fast terminal sliding mode can ensure that the system reaches the sliding mode surface and the system state quickly converges to an equilibrium state. According to the sliding surfaces of the lower layer, the equivalent input in the sense of Filippov[33] is obtained, and the switching function is obtained using the feedback function[34] for the sliding surface of the upper layer. After the integration of the equivalent input terms and the switching control function term, the total system input that can ensure the stability of the overall sliding surface is obtained.

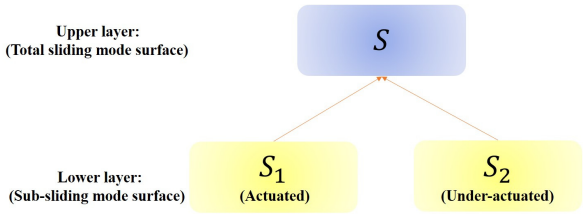


**Fig. 2:** Schematic diagram of Hierarchical sliding mode

### 3.1 Selection of target trajectory

In order to realize the stable control of the bridge crane system, a smooth s-shaped curve is used for the track of the vehicle. In this paper, the target trajectory of the trolley is designed by Fang et al[35]. in the adaptive trajectory tracking and anti-pendulum control of 2D 2-dof bridge crane system model, which is given by

$$\begin{aligned} x_d =& \frac{P_{dx}}{2} + \frac{k_{vx}^2}{4k_{ax}} \ln(\cosh(2k_{ax}t/k_{vx} - \varepsilon_x) \\ & / \cosh(2k_{ax}t/k_{vx} - \varepsilon_x - 2P_{dx}k_{ax}/k_{vx}^2)), \\ y_d =& \frac{P_{dy}}{2} + \frac{k_{vy}^2}{4k_{ay}} \ln(\cosh(2k_{ay}t/k_{vy} - \varepsilon_y) \\ & / \cosh(2k_{ay}t/k_{vy} - \varepsilon_y - 2P_{dy}k_{ay}/k_{vy}^2)). \end{aligned} \tag{20}$$

where $x_d$ and $y_d$ are target trajectory, $P_dx$ and $P_dy$ are target position of the vehicle, $k_vx$ and $k_vy$ are maximum speed of the vehicle, $k_ax$ and $k_ay$ are maximum acceleration of the vehicle, $\varepsilon_x$ and $\varepsilon_y$ are initial acceleration parameter of the vehicle, $t$ is time.

### 3.2 Error function deformation

Considering the model defined by Eqn.(18), the input of the system are $f_x$ and $f_y$; hence, the number of inputs is $n_i = 2$. Clearly, the number of degrees of freedom of the crane system is $n = 4$.

Set the target values of the swing angles $\theta_x$ and $\theta_y$ to 0, then the target state vector of the system is given by

$$q_d = \begin{bmatrix} x_d & y_d & 0 & 0 \end{bmatrix}^T. \tag{21}$$

The dynamic equation of bridge crane system is transformed into error state equation, which is given by

$$\begin{aligned} M(q)(\ddot{q} - \ddot{q}_d) + \bar{C}(q,\dot{q})(\dot{q} - \dot{q}_d) = F - G(q) \\ - M(q)\ddot{q}_d - \bar{C}(q,\dot{q})\dot{q}_d. \end{aligned} \tag{22}$$

We denote that

$$\begin{aligned} e &= q - q_d, \\ &= \begin{bmatrix} x - x_d & y - y_d & \theta_x & \theta_y \end{bmatrix}^T, \\ &= \begin{bmatrix} e_x & e_y & e_{\theta x} & e_{\theta y} \end{bmatrix}^T. \end{aligned} \tag{23}$$

$$\begin{aligned} U &= F - G(q) - M(q)\ddot{q}_d - \bar{C}(q,\dot{q})\dot{q}_d, \\ &= \begin{bmatrix} \sigma_x & \sigma_y & \sigma_{\theta x} & \sigma_{\theta y} \end{bmatrix}^T. \end{aligned} \tag{24}$$

where

$$\begin{aligned} \sigma_x &= f_x - (M_x + m)\ddot{x}_d - D_x\dot{x}_d, \\ \sigma_y &= f_y - (M_y + m)\ddot{y}_d - D_y\dot{y}_d, \\ \sigma_{\theta x} &= -mgl\sin\theta_x\cos\theta_y - m\ddot{x}_d l\cos\theta_x\cos\theta_y, \\ \sigma_{\theta y} &= -mgl\cos\theta_x\sin\theta_y + m\ddot{x}_d l\sin\theta_x\sin\theta_y \\ &\quad - m\ddot{y}_d l\cos\theta_y. \end{aligned} \tag{25}$$

By using Eqn.(23), Eqn.(24) and Eqn.(25), Eqn.(18) can be writen as follows:

$$M(q)\ddot{e} + \bar{C}(q,\dot{q})\dot{e} = U. \tag{26}$$

### 3.3 Hierarchical global fast terminal sliding mode controller design

The error equation of state of the bridge crane system in Eqn.(26) can be writern as follows:

$$\ddot{e} = M^{-1}(q)[U - \bar{C}(q,\dot{q})\dot{e}]. \tag{27}$$

To further solve the controller equation, these parameters are defined

$$\begin{aligned} e_p = \begin{bmatrix} e_x & e_y \end{bmatrix}^T, e_\theta = \begin{bmatrix} e_{\theta x} & e_{\theta y} \end{bmatrix}^T, \\ \sigma_p = \begin{bmatrix} \sigma_x & \sigma_y \end{bmatrix}^T, \sigma_\theta = \begin{bmatrix} \sigma_{\theta x} & \sigma_{\theta y} \end{bmatrix}^T, \end{aligned} \tag{28}$$

and

$$M^{-1}(q) = \begin{bmatrix} \Pi_{11} & \Pi_{12} \\ \Pi_{21} & \Pi_{22} \end{bmatrix}, \tag{29}$$

where $\Pi_{11}$, $\Pi_{12}$, $\Pi_{21}$ and $\Pi_{22}$ are all second order matrices. At the same tinme, make $\Pi_1 = \begin{bmatrix} \Pi_{11} & \Pi_{12} \end{bmatrix}$, $\Pi_2 = \begin{bmatrix} \Pi_{21} & \Pi_{22} \end{bmatrix}$.

Substituting the above equation into Eqn.(27)

$$\begin{aligned} \ddot{e}_p &= \Pi_{11}\sigma_p + \Pi_{12}\sigma_\theta - \Pi_1 C(q,\dot{q})\dot{e}, \\ \ddot{e}_\theta &= \Pi_{21}\sigma_p + \Pi_{22}\sigma_\theta - \Pi_2 C(q,\dot{q})\dot{e}. \end{aligned} \tag{30}$$

The sliding surface of the lower layer is designed for the displacement error of the vehicle and the swing angle error of the lifting payload:

$$\begin{aligned} S_1 &= \dot{e}_p + H_1 e_p + \alpha e_p^{n/p}, \\ S_2 &= \dot{e}_\theta + H_2 e_\theta + \beta e_\theta^{n/p}. \end{aligned} \tag{31}$$

where, $H_1 = \begin{bmatrix} H_{1x} & 0 \\ 0 & H_{1y} \end{bmatrix}$, $H_2 = \begin{bmatrix} H_{2\theta_x} & 0 \\ 0 & H_{2\theta_y} \end{bmatrix}$, and designed parameters $\alpha$, $\beta$, $H_{1x}$, $H_{1y}$, $H_{2\theta_x}$, $H_{2\theta_y}$ are all positive constants, $n$ and $p$ are positive odds.

According to the Filippov equivalence theory[36], we can know

$$\begin{aligned}\dot{S}_1 &= \ddot{e}_p + H_1\dot{e}_p + \alpha(n/p)e_p^{n/p-1} = 0,\\ \dot{S}_2 &= \ddot{e}_\theta + H_2\dot{e}_\theta + \beta(n/p)e_\theta^{n/p-1} = 0.\end{aligned} \tag{32}$$

The equivalent sliding mode control input of the sub-system is given by bringing Eqn.(32) into Eqn.(30)

$$\begin{aligned}\sigma_1 &= -\Pi_{11}^{-1}[\Pi_{12}\sigma_\theta - \Pi_1 C(q,\dot{q})\dot{e} + H_1\dot{e}_p + \alpha(n/p)e_p^{n/p-1}],\\ \sigma_2 &= -\Pi_{21}^{-1}[\Pi_{22}\sigma_\theta - \Pi_2 C(q,\dot{q})\dot{e} + H_2\dot{e}_\theta + \beta(n/p)e_\theta^{n/p-1}].\end{aligned} \tag{33}$$

The upper layer total sliding surface is defined as

$$S = I_1 S_1 + I_2 S_2. \tag{34}$$

where,$I_1 = \begin{bmatrix} i_{1x} & 0 \\ 0 & i_{1y}\end{bmatrix}, I_2 = \begin{bmatrix} i_{2\theta_x} & 0 \\ 0 & i_{2\theta_y}\end{bmatrix}$, and designed parameters $i_{1x}, i_{1y}, i_{2\theta_x}, i_{2\theta_y}$ are all positive constants.

Since the number of input control quantities of the under-actuated system is less than the number of output quantities that need to be controlled. Thus, even if each sub-system is guaranteed to move towards its own sliding surface, this does not apply to the entire system. If the total control input only includes the equivalent parts and the switching function part of each sub-system, it cannot ensure that the total system will reach the total sliding surface in a limited time. In other words, it is necessary to make each sub-sliding a die surface in order to ensure the stability of the overall sliding die surface, so the following total system input is defined

$$\sigma_{total} = \sigma_1 + \sigma_2 + \sigma_{sw}, \tag{35}$$

where $\sigma_{sw}$ is switch term.

For the convenience of the subsequent derivation process, Eqn.(27) is changed into the following form

$$\begin{aligned}\ddot{e}_p &= A_1(e) + B_1(e)U,\\ \ddot{e}_\theta &= A_2(e) + B_2(e)U.\end{aligned} \tag{36}$$

where $\begin{bmatrix} A_1(e) \\ A_2(e)\end{bmatrix} = \left[-M^{-1}(q)\bar{C}(q,\dot{q})\right], \begin{bmatrix} B_1(e) \\ B_2(e)\end{bmatrix} = \left[M^{-1}(q)\right]$, $A_1(e), A_2(e), B_1(e), B_2(e) \in \mathbb{R}^{2\times 4}$.

The sliding mode controller is designed by using Lyapunov feedback function. Firstly, a positive definite Lyapunov function $V = S^2/2$ is defined,

Take the derivative of both sides of the Lyapunov function with respect to time, the follow equation can be obtained

$$\begin{aligned}\dot{V} =& S\dot{S}\\ =& S(I_1\dot{S}_1 + I_2\dot{S}_2)\\ =& S[I_1(\ddot{e}_p + H_1\dot{e}_p + \alpha(n/p)e_p^{n/p-1})\\ &+ I_2(\ddot{e}_\theta + H_2\dot{e}_\theta + \beta(n/p)e_\theta^{n/p-1})]\\ =& S[I_1(H_1\dot{e}_p + \alpha(n/p)e_p^{n/p-1} + (A_1(e) + B_1(e)U))\\ &+ I_2(H_2\dot{e}_\theta + \beta(n/p)e_\theta^{n/p-1} + (A_2(e) + B_2(e)U))]\\ =& S[I_2\Pi_{21}\sigma_1 + I_1\Pi_{11}\sigma_2 + \alpha(n/p)e_p^{n/p-1}\\ &+ \beta(n/p)e_\theta^{n/p-1} + (I_1\Pi_{11} + I_2\Pi_{21})\sigma_{sw}].\end{aligned} \tag{37}$$

please refer to the Appendix 2 for details.

The exponential approach is taken as follows

$$\begin{aligned}\dot{S} &= -WS - K\mathrm{sgn}(S)\\ &= I_2\Pi_{21}\sigma_1 + I_1\Pi_{11}\sigma_2 + \alpha(n/p)e_p^{n/p-1}\\ &+ \beta(n/p)e_\theta^{n/p-1} + (I_1\Pi_{11} + I_2\Pi_{21})\sigma_{sw}.\end{aligned} \tag{38}$$

where $W = \begin{bmatrix} \omega_{3x} & 0 \\ 0 & \omega_{3y}\end{bmatrix}, K = \begin{bmatrix} k_{4x} & 0 \\ 0 & k_{4y}\end{bmatrix}$, and designed parameters $\omega_{3x}$ , $\omega_{3y}$, $k_{4\theta_x}$, $k_{4\theta_y}$ are all positive constants.

It can be obtained from Eqn.(38) that

$$\begin{aligned}\sigma_{sw} =& -(I_1\Pi_{11} + I_2\Pi_{21})^{-1}[I_2\Pi_{21}\sigma_1\\ &+ I_1\Pi_{11}\sigma_2 + \alpha(n/p)e_p^{n/p-1}\\ &+ \beta(n/p)e_\theta^{n/p-1} + WS + K\mathrm{sgn}(S)].\end{aligned} \tag{39}$$

Substituting Eqn.(39) into Eqn.(63)

$$\begin{aligned}\dot{V} &= S[-WS - K\mathrm{sgn}(S)]\\ &= -SWS - SK\mathrm{sgn}(S) \le 0.\end{aligned} \tag{40}$$

If and only if $S = 0$, the equal sign is true. So the whole system is stable.

So the total input to the system is given as follows

$$\begin{aligned}\sigma = \begin{bmatrix} \sigma_x \\ \sigma_y\end{bmatrix} &= \sigma_1 + \sigma_2 + \sigma_{sw}\\ =&(I_1\Pi_{11} + I_2\Pi_{21})^{-1}[I_1\Pi_{11}\sigma_1 + I_2\Pi_{21}\sigma_2 -\\ &\alpha(n/p)e_p^{n/p-1} - \beta(n/p)e_\theta^{n/p-1} - WS - K\mathrm{sgn}(S)].\end{aligned} \tag{41}$$

Then, the control input of the system which is given in Eqn.(18) is obtained as follows

$$\begin{aligned}f_x &= \sigma_x + (M_x + m)\ddot{x}_d + D_x\dot{x}_d,\\ f_y &= \sigma_y + (M_y + m)\ddot{y}_d + D_y\dot{y}_d.\end{aligned} \tag{42}$$

## 4 Stability analysis

If all the sliding surfaces of a system are Lyapunov stable, at the same time they are all asymptotically stable, then the asymptotically stable system can reach equilibrium, so the stability and controllability of the system must be demonstrated.

### *4.1 Proof of the asymptotic stability of the total sliding surface of the system*

*Lemma* 1*:* $\forall t \ge 0, \forall t_1 \ge 0$, we suppose $0 \le t < t_1$, there must be a certain $t_2 \in (t, t_1)$, then you can get a conclusion that $\dot{S}_t - \dot{S}_{t_1} = \ddot{S}_{t_2}(t - t_1)$. Supposing the upper bound of $\left|\ddot{S}\right|$ is $\hat{\varepsilon} > 0$, let $\psi(\varepsilon) = \varepsilon/\hat{\varepsilon} > 0$. When if fills $|t - t_1| < \psi$, the equation $\left|\dot{S}_t - \dot{S}_{t_1}\right| = \left|\ddot{S}_{t_2}\right| |t - t_1| \le \hat{\varepsilon}\,|t - t_1| < \hat{\varepsilon}(\varepsilon/\hat{\varepsilon}) = \varepsilon$ must be satisfied.

According to Babarlat's Lemma[37], the following three conditions are proposed

1) $S$ is a differentiable function, and $S$ is bounded.
2) $\dot{S}$ is a differentiable function, and $\dot{S}$ is bounded. $\dot{S}$ is also uniformly continuous in the interval $t \in [0, \infty)$.
3) $\ddot{S}$ is bounded.

*Theorem* 1*:* If $S$ meets the above three conditions can be proved, then it is easy to get the conclusion of $\lim_{t\to\infty} \dot{S} = 0$.

*Proof:* Accroding to Lemma 1 we can know $\dot{S}$ is uniformly continuous in the interval $t \in [0, \infty)$ which is mentioned in condition 2. Next we prove the other parts of the above three conditions.

The Lyapunov function is redefined for the total sliding surface for the convenience of writing as follows

$$V_i = \frac{1}{2} S_i^2 \, (i = x, y) \, . \tag{43}$$

Considering whether it is $S_x$ or $S_y$, its proof process is the same, so $S_x$ is taken as an example.

From Eqn.(38)

$$\dot{S}_x = -\omega_{3x} S_x - k_{4x} \mathrm{sgn}(S_x). \tag{44}$$

By Eqn.(40), the derivative of $V_x$ is given by

$$\dot{V}_x = S_x \dot{S}_x = -\omega_{3x} S_x^2 - k_{4x} \left| S_x \right| . \tag{45}$$

Obviously, $\dot{V}_x \leq 0$ is satisfied, if and only if $S_x = 0$, the equal sign can be true.

Integrate both sides of Eqn.(45) at the same time

$$\int_0^t \dot{V}_x d\sigma = \int_0^t -\omega_{3x} S_x^2 - k_{4x} \left| S_x \right| d\sigma. \tag{46}$$

The above equation can be wirtten as

$$V_x = V_x(0) + \int_0^\infty -\omega_{3x} S_x^2 - k_{4x} \left| S_x \right| d\sigma. \tag{47}$$

It can be concluded from the above equation that

$$V_x \leq V_x(0) - \int_0^\infty \omega_{3x} S_x^2 + k_{4x} \left| S_x \right| d\sigma < V_x(0). \tag{48}$$

According to the definition of the function $V_x$ and the definition of the sliding surface function, we can get $0 < V_x(0) = \frac{1}{2} S_x^2(0)$. Because $S_x(0) = I_1 S_1(0) + I_2 S_2(0) = I_1[\dot{e}_p(0) + H_1 e_p(0) + \alpha e_p^{n/p}(0)] + I_2[\dot{e}_\theta(0) + H_2 e_\theta(0) + \beta e_\theta^{n/p}(0)] < \infty$.

So

$$0 < V_x(t) = \frac{1}{2} S_x^2 < V_x(0) < \infty. \tag{49}$$

Obviously, $S_x \in L_\infty$.

By Eqn.(40)

$$\dot{V}_x = S_x \dot{S}_x = -S_x W S_x - S_x K \mathrm{sgn}(S) \leq 0. \tag{50}$$

We already proved that $S_x \in L_\infty$, if $\dot{S}_x \notin L_\infty$, the product of $S_x$ and $\dot{S}_x$ can't have an upper bound of 0. So, we can get the conclusion $\dot{S}_x \in L_\infty$. Which means $\dot{S}_x$ is a differentiable function, and $\dot{S}_x$ is bounded.

By Eqn.(48) and Eqn.(49), we can know that

$$0 \leq V_x(0) - \int_0^\infty \omega_{3x} S_x^2 + k_{4x} \left| S_x \right| d\sigma. \tag{51}$$

The above equation can be written as

$$\int_0^\infty \omega_{3x} S_x^2 + k_{4x} \left| S_x \right| d\sigma < V_x(0) < \infty. \tag{52}$$

By Eqn.(52), the sum of two positive factors is less than infinity, so that neither of these positive factors can go to infinity. Otherwise, the above equation is not true. So we can get that

$$\begin{aligned} &\int_0^\infty \omega_{3x} S_x^2 d\sigma < \infty, \\ &\int_0^\infty k_{4x} \left| S_x \right| d\sigma < \infty. \end{aligned} \tag{53}$$

where $\omega_{3x}$ and $k_{4x}$ are both constants greater than zero, so $S$ is absolutely integrable and square integrable. Therefore, we can get $S_x \in L_1$ and $S_x \in L_2$. Which means $S_x$ is a differentiable function, and $S_x$ is bounded.

So far, the three conditions in *Theorem* 1 have been verified, and we have $\lim_{t \to \infty} \dot{S}_x = 0$.

*Theorem 2:* The limit of the total sliding surface function of the system as time approaches infinity is 0, $\lim_{t \to \infty} S_x = 0$.

*Proof:* We assume that $\lim_{t \to \infty} S_x = C \neq 0$. In *Theorem* 1, we already have $\lim_{t \to \infty} \dot{S}_x = 0$, so that $\int_0^\infty S_x^2 d\sigma = \Omega + \int_t^\infty C^2 d\sigma$, where $\Omega$ means $\int_0^t S_x^2 d\sigma$,we denote $\forall T > t, \dot{S}_x = 0$. Because $S_x \in L_1$, that is $\sup_{t \geq 0} |S_x| = ||S_x||_\infty < \infty$, the definite integral of its square function must also be less than infinity. So we have $\Omega = \int_0^t S_x^2 d\sigma < \infty$. obviously, $\lim_{t \to \infty} \int_t^\infty C^2 d\sigma = \infty$ is true. So that $\lim_{t \to \infty} \int_0^\infty S_x^2 d\sigma = \lim_{t \to \infty} (\Omega + \int_t^\infty C^2 d\sigma) = \infty$ either must be true. This contradicts $\int_0^\infty S_x^2 d\sigma < \infty$, which has been proved above, so the assumption is not true. There must be $\lim_{t \to \infty} S_x = 0$.

It is easy to conclude that the total sliding surface of the system is not only Lyapunov stable but also asymptotically stable.

### *4.2 Proof of asymptotic stability of the subslip surface of the system*

By Eqn.(31), the two sub-sliding surfaces are respectively $S_1$ and $S_2$. For the bridge crane system, the equilibrium point of the system is obviously the stable equilibrium point. Therefore, we simulate the method of proving the stability of the total sliding surface to prove the stability of the sub-sliding surface.

It has been said before that the equilibrium point of the bridge crane system is the stable equilibrium point. That is to say, there is a field at the equilibrium point $x_0$, and all trajectories in this neighborhood will eventually approach the equilibrium point rather than towards infinity. Since it is so, $S_1 \in L_\infty$ and $\dot{S}_1 \in L_\infty$ are easy to get, which can be written as

$$\begin{aligned} &\sup_{t \geq 0} |S_1| = ||S_1||_\infty < \infty, \\ &\sup_{t \geq 0} \left| \dot{S}_1 \right| = \left|\left| \dot{S}_1 \right|\right|_\infty < \infty. \end{aligned} \tag{54}$$

By Eqn.(34), it is easy to get that

$$\sup_{t \geq 0} |S| = ||S||_\infty \leq ||I_1 S_1||_\infty + ||I_2 S_2||_\infty. \tag{55}$$

If the right end of the above formula goes to infinity, that is to say $||I_2 S_2||_\infty \underset{t \to \infty}{\to} 0$. In other words, when the system's running time tends to infinity, when the asymptotically stable total sliding surface function reaches zero, and when there is an actuated sub-system that converges towards a small neighborhood near the equilibrium point, the under-actuated sub-systems tend to be infinite. This is clearly unreasonable. Therefore, the sliding surface function $S_2$ of the under-actuated sub-system must also satisfy the following equation

$$\begin{aligned} &\sup_{t \geq 0} |S_2| = ||S_2||_\infty < \infty, \\ &\sup_{t \geq 0} \left| \dot{S}_2 \right| = \left|\left| \dot{S}_2 \right|\right|_\infty < \infty. \end{aligned} \tag{56}$$

The following equations are going to be given

$$\begin{aligned} &S_1 \in L_\infty, \dot{S}_1 \in L_\infty, \\ &S_2 \in L_\infty, \dot{S}_2 \in L_\infty. \end{aligned} \tag{57}$$

It is easy to know $S_1 \in L_1$, by Eqn.(53)

$$\int_0^\infty |S| d\sigma \leq \int_0^\infty (I_1 |S_1| + I_2 |S_2|) d\sigma. \tag{58}$$

In a similar way, if the right end of this goes to infinity, then $\int_0^\infty I_2 |S_2| d\sigma \to \infty$, so we can figure out the sliding surface function $S_2$ of under-actuated sub-system must satisfy $S_2 \in L_1$.

By Eqn.(57) and $S_1 \in L_1$, we can know $\int_0^\infty |S_1| d\sigma < \infty$, that is to say $\sup_{t \geq 0} |S_1| = ||S_1||_\infty < \infty$. At the same time, on the basis of $\int_0^\infty S_1^2 d\sigma = \int_0^\infty |S_1| \cdot |S_1| \, d\sigma \leq \int_0^\infty ||S_1||_\infty \cdot |S_1| \, d\sigma \leq ||S_1||_\infty \int_0^\infty |S_1| \, d\sigma < \infty$, it can be given as

$$\int_0^\infty S_1^2 d < \infty. \tag{59}$$

In a similar way, we can know

$$\int_0^\infty S_2^2 d\sigma < \infty. \tag{60}$$

whcih can be writen as $S_1 \in L_2$ and $S_2 \in L_2$.

In conclusion, this article has proved $S_1 \in L_1$, $S_1 \in L_2$, $S_1 \in L_\infty$, $\dot{S}_1 \in L_\infty$ and $S_2 \in L_1$, $S_2 \in L_2$, $S_2 \in L_\infty$, $\dot{S}_2 \in L_\infty$ in turn.

By Eqn.(52) and Eqn.(53), same as the proof process in the previous section, these conclusions will be given as follows

$$\begin{aligned} &\lim_{t \to \infty} \dot{S}_1 = 0, \lim_{t \to \infty} \dot{S}_2 = 0, \\ &\lim_{t \to \infty} S_2 = 0, \lim_{t \to \infty} S_2 = 0. \end{aligned} \tag{61}$$

The above equation proves that the two sub-sliding surfaces of the system are not only stable but also asymptotically stable.

In summary, this paper proves the asymptotic stability of all sliding surfaces of the system, and shows that the controller can drive the system to the sliding surface in finite time and finally stabilize at the target position.

## 5 Simulation and analysis

Several simulations have been undertaken which are concerned with the 3D bridge crane system given by Eqn.(8)-(11) controlled using the H-GFTSMC given by Eqn.(42). The controller parameters used in the simulations are selected as

$$\begin{aligned} &H_1 = \begin{bmatrix} 0.8 & 0 \\ 0 & 0.8 \end{bmatrix}, H_2 = \begin{bmatrix} 0.4 & 0 \\ 0 & 0.016 \end{bmatrix}, \\ &I_1 = \begin{bmatrix} 9 & 0 \\ 0 & 84 \end{bmatrix}, I_2 = \begin{bmatrix} 12 & 0 \\ 0 & 110 \end{bmatrix}, \\ &W = \begin{bmatrix} 10 & 0 \\ 0 & 50 \end{bmatrix}, K = \begin{bmatrix} 0.03 & 0 \\ 0 & 0.028 \end{bmatrix}. \end{aligned} \tag{62}$$

Some other related parameters are given by $g = 9.81\text{m/s}^2$, $m = 30\text{kg}$, $M_x = 1440\text{kg}$, $M_y = 110\text{kg}$, $D_x = 480\text{kg/s}$, $D_y = 40\text{kg/s}$, $P_{dx} = 50\text{m}$, $P_{dy} = 20\text{m}$, $k_{ax} = 0.25\text{m/s}^2$, $k_{ay} = 0.08\text{m/s}^2$, $k_{vx} = 1.05\text{m/s}$, $k_{vy} = 0.53\text{m/s}$, $\varepsilon_x = \varepsilon_y = 2.5$, $l = 10\text{m}$, $\alpha = 1$, $\beta = 0.5$, $n = 1$, $p = 5$.

The initial positions are taken to be $(x_0, y_0, \theta_{x0}, \theta_{y0}) = (0, 0, 0, 0)$ while the desired values are chosen to be $(x_d, y_d, \theta_{xd}, \theta_{yd}) = (50, 20, 0, 0)$.

According to the above parameters, the bridge crane system is simulated. The simulation results are analyzed below.

### 5.1 Simulation on H-GFTSMC performance

Fig.3 shows the track of the trolley and the swing angle diagram of the lifting payload.

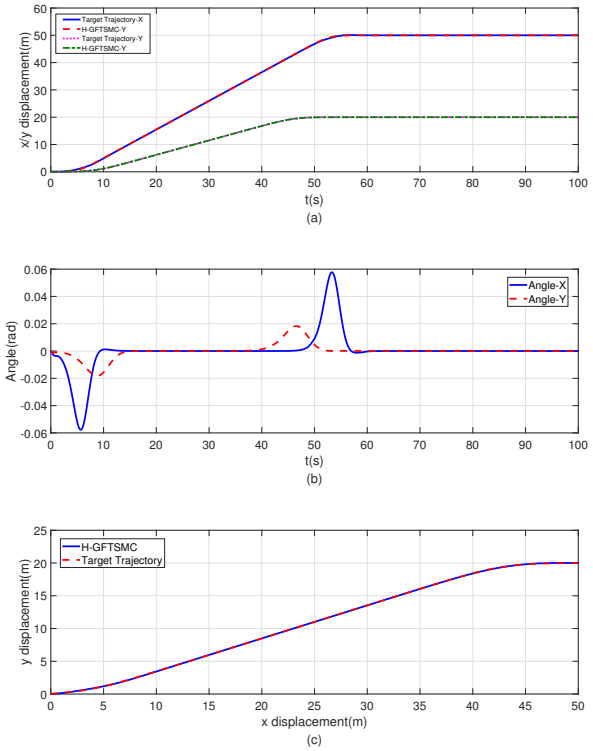


**Fig. 3:** Overall control renderings: track of the trolley and its target track(a), angular component of the payload suspended in the X and Y directions(b), top view of spatial displacement of the vehicle(c)

It can be seen in Fig.3(a) and Fig.3(c), the displacement trajectory of the vehicle is basically consistent with the target trajectory. It can also been in Fig.3(b) that the swing angle of the lifting payload has almost no swing outside the start and stop time. When the crane starts, the angle of the pendulum in the X direction reaches its maximum value of $-0.06$rad in about 5s. Meanwhile, the angle of the pendulum in the Y direction reaches the maximum value of $-0.018$rad in about 9s. When the crane stops, the angles in X and Y direction reach the maximum value of $0.058$rad and $0.019$rad in about 54s and 48s, respectively. Outside these two time periods, the angle decays rapidly to zero. Under the control of H-GFTSMC, the displacement tracking of the trolley is good, and the pendulum angles in both X and Y directions are limited to a small range.

Next, the simulation results of controller stability are analyzed. The results are shown in the following figures.

All the sliding surfaces of the entire system are shown in Fig.4, where Fig.4(a) and Fig.4(b) show the displacement dependent sub-sliding surface and the pendulum angle dependent sub-sliding surface, respectively. During the process of starting and stopping of bridge crane system, each sub-sliding surface will fluctuate, but it will converge to 0 soon. It can be seen from Fig.4(a) and Fig.4(b) that the two sub-sliding surfaces enter the sliding mode movement soon after the simulation starts, and then stabilize near the designed sliding surface. It can be seen from Fig.4(c) that the total sliding surface of the system is stable near 0 except for the start and stop phases. Hence, the simulation results verify the asymptotic stability of the designed hierarchical global fast terminal sliding mode controller.

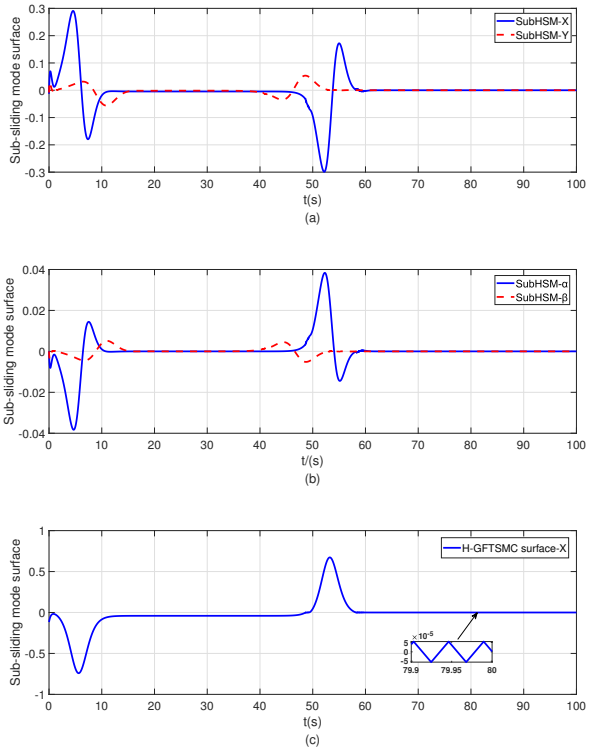


**Fig. 4:** All sliding mode surfaces:The sub-sliding surface of the displacement-dependent sub-system(a), sub-sliding surface of the sub-system related to the pendulum angle(b), total sliding surface of the whole system(c)

### 5.2 *Simulation on comparation with PID*

In order to show the superiority of the proposed control method, its control performance is compared with the traditional PID control method and the simulation results are as follows.

Because of the controller design process of the vehicle in X and Y directions is the same, the motion in the x direction is analyzed separately with PID.

Fig.5 shows the comparison of control performance of cart under H-GFTSMC and PID controllers. It can be seen from Fig.5(a) that the performance of trajectory tracking under the H-GFTSMC is excellent. The cart basically runs along the planned trajectory, and there is almost no overshooting when it stops. However, under the traditional PID control, the responding speed of cart is slow, and certain overshoot occurs when stopping. In Fig.5(b), the payload swings slightly at start and stop, and returns to 0 rapidly in the rest of the time. In contrast, the pendulum angle under the PID control is slightly lower than that under the H-GFTSMC control, but there is always a certain pendulum angle during operation process. Therefore, H-GFTSMC method has obvious advantages compared with the traditional PID control method.

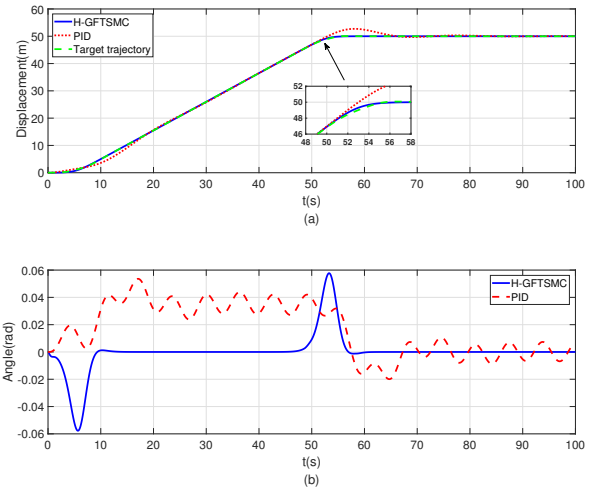


**Fig. 5:** Comparison of the displacement(a), comparison of the angles(b)

### 5.3 *Simulation on robustness when changing the length of the cable*

Next, the controller robustness is simulated and analyzed. The robustness is verified by changing the length of the hanging cable. Fig.6 and Fig.7 show the simulation results of increasing and decreasing the length of hoisting cable respectively.

The cable length of the controller is set to 10m, on the other side, the actual cable lenth is set to be 5m and 15m.

Comparing with Fig.6(a) and Fig.3(a), the curve fluctuation in Fig.6(a) does not increase significantly. Even if the cable length is shortened, the controller can still obtain a better displacement tracking performance. It can also be seen from Fig.6(b) and Fig.3(b), there is no significant swing amplitude change in the swing angle of the lifting payload, and the anti-swing control performance is

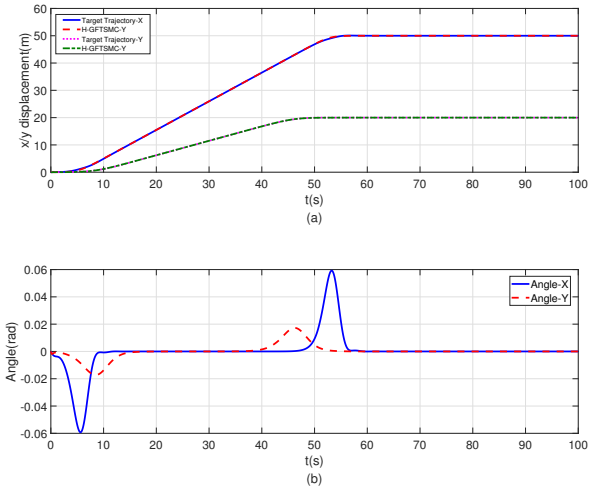


**Fig. 6:** The performance of shortening the length of hanging cable on the displacement(a) and angles(b)

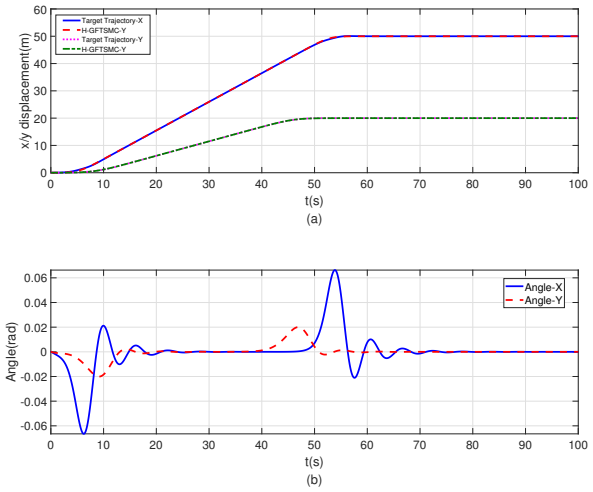


**Fig. 7:** The performance of longering the length of hanging cable on the displacement(a) and angles(b)

still good. Therefore, when the cable length is shortened, the control performance of the controller is still considerable.

When the cable length is increased, the displacement tracking performance is good, with no large tracking error as shown in Fig.7(a) and Fig.3(a). However, there are some problems with the angle. As shown in Fig.7(b), when the crane starts and stops, the pendulum angle has some small fluctuations and is unable to return to 0 quickly.

### *5.4 Simulation on adding white noise*

All above simulations are conducted under the ideal conditions. Due to issues such as sensor accuracy, there must be a lot of noise that cannot be ignored in the process of system operation. Therefore, on the basis of the first simulation, Gaussian white noise is added to the feedback collected by the system to verify the robustness of the proposed control method proposed in the presence of interference. The simulation results are shown in Fig.8.

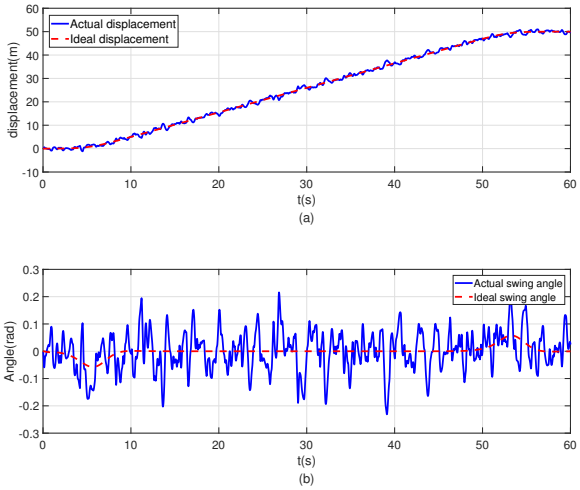


**Fig. 8:** The effect of white noise on the displacement(a) and angles(b)

In Fig.8(a), the blue curve and the red dotted line represent the actual and the ideal trajectories of the cart, respectively. It can be observed that the actual trajectory of the cart swings around the ideal trajectory and the swing amplitude is small. Fig.8(b) shows the comparison between the actual swing and the ideal swing angles. In the actual simulation, although the swing frequency is high, the swing amplitude is still limited to a small range.

## 6 Conclusion

In this paper, a H-GFTSMC is proposed to handle the problem of large payload swing during the operation of the bridge crane system. Firstly, the Lagrangian dynamic modeling of the bridge crane system is been conducted. Then, the hierarchical sliding mode controller is designed according to the under-actuated characteristics of the system. The stability of the proposed controller is verified, and it is proved that all sliding surfaces of the controller tend to be gradually stable. Finally, the simulation results demonstrate that the controller has a good restraining preformance on the swing angle of the payload, and at the same time, the controller still has good robustness when the cable length is changed. Moreover, the performance of the controller is still excellent even when the feedback signal contains noise.

## 7 References


1 d' Andréa.Novel, B., Coron, J.M.: 'Exponential stabilization of an overhead crane with flexible cable via a back-stepping approach', Automatica, 2000, 36, (4), pp. 587–593

2 Manson, G.A.: 'Time-optimal control of an overhead crane model', 1982, 3, (2), pp. 115–120

3 Manson, G.A.: 'Time-optimal control of an overhead crane model', Optimal Control Applications & Methods, 1982, 3, (2), pp. 115–120

4 Mansour.A..Karkoub, M.A.K.: 'Robust control schemes for an overhead crane', Journal of Vibration and Control, 2001, 7, (3), pp. 395–416

5 Nourollahi.Darabad, M., Mazloumi, A., Saraji, G.N., Afshari, D., Foroushani, A.R.: 'Full shift assessment of back and head postures in overhead crane operators with and without symptoms', Journal of Occupational Health, 2018, 60, (1), pp. 46–54

6 Zhao, Y., Gao, H.: 'Fuzzy-model-based control of an overhead crane with input delay and actuator saturation', IEEE Transactions on Fuzzy Systems, 2012, 20, (1), pp. 181–186

7 Srivastava, N.K., Mondal, S.: 'Development of predictive maintenance model of an overhead crane exercising nhpp models', IAENG International Journal of Computer Science, 2014, 13, (3), pp. 71

8 Moustafa, K.A.F., Ebeid, A.M.: 'Nonlinear modeling and control of overhead crane load sway', Transaction of the Asme Journal of Dynamic Systems Measurement & Control, 1988, 110, (3), pp. 266–271

9 Lee, H.H.: 'Modeling and control of a three-dimensional overhead crane', Journal of Dynamic Systems, Measurement, and Control, 1998, 120, (4), pp. 471–476

10 Liu, R., Li, S., Ding, S.: 'Nested saturation control for overhead crane systems', Transactions of the Institute of Measurement & Control, 2012, 34, (7), pp. 862–875

11 Nguyen, H.T.: 'State-variable feedback controller for an overhead crane', Journal of Electrical & Electronics Engineering, 1994, 14, (2), pp. 75–84

12 Mahfouf, M., Kee, C.H., Abbod, M.F., Linkens, D.A.: 'Fuzzy logic-based antisway control design for overhead cranes', Neural Computing and Applications, 2000, 9, (1), pp. 38–43

13 Yoshida, Y., Tabata, H.:'Visual feedback control of an overhead crane and its combination with time-optimal control'. In: IEEE/ASME International Conference on Advanced Intelligent Mechatronics. Xian, China, jul 2008. pp. 1114–1119

14 Yang, J.H., Shen, S.H.:'A novel approach for the adaptive tracking control for 3-d overhead crane system'. In: International Conference on Modelling. Shanghai, China, Jun 2008. pp. 446–450

15 Soukkou, A., Khellaf, A., Leulmi, S.:'Control of overhead crane by fuzzy-pid with genetic optimisation'. In: Ifip International Conference on Artificial Intelligence Applications & Innovations. Springer, Boston, MA, 2004. pp. 67–80

16 Ko, C.N.: 'A Fuzzy PID Controller Based on Hybrid Optimization Approach for an Overhead Crane'. (Springer Berlin Heidelberg, 2011)

17 Choi, Y.: 'Pid state estimator for lagrangian systems', IET Control Theory & Applications, 2007, 1, (4), pp. 937–945

18 Cuoghi, Stefania, Ntogramatzidis, Lorenzo: 'Direct and exact methods for the synthesis of discrete-time proportional-integral-derivative controllers.', IET Control Theory & Applications, 2013, 7, (18), pp. 2164–2171

19 Ahmad, M., A., Saealal, M., S., et al.: 'Single input fuzzy controller with command shaping schemes for double-pendulum-type overhead crane.', AIP Conference Proceedings, 2011, 1337, (1), pp. 1397–1402

20 Konstantopoulos, G.C., Alexandridis, A.T.:'Simple energy based controllers with nonlinear coupled-dissipation terms for overhead crane systems'. In: IEEE Conference on Decision & Control. Shanghai, China, Dec 2009. pp. 3149–3154

21 Mendez, J.A., Acosta, L., Moreno, L., Hamilton, A.:'Design of a neural network based self-tuning controller for an overhead crane'. In: IEEE International Conference on Control Applications. Trieste, Italy, Sept 1998. pp. 168–171

22 Petrenko, Y.N., Alavi, S.E.:'Fuzzy logic and genetic algorithm technique for nonliner system of overhead crane'. In: IEEE Region 8 International Conference on Computational Technologies in Electrical & Electronics Engineering. Listvyanka, Russia, July 2010. pp. 848–851

23 Zhu, X., Wang, N.: 'Cuckoo search algorithm with membrane communication mechanism for modeling overhead crane systems using rbf neural networks', Applied Soft Computing, 2017, 56, pp. 458–471

24 Jahedi, G., Ardehali, M.M.: 'Genetic algorithm-based fuzzy-pid control methodologies for enhancement of energy efficiency of a dynamic energy system', Energy Conversion & Management, 2011, 52, (1), pp. 725–732

25 Wang, W., Liu, X.D., Yi, J.Q.: 'Structure design of two types of sliding-mode controllers for a class of under-actuated mechanical systems', IET Control Theory & Applications, 2007, 1, (1), pp. 163–172

26 Liu, D., Yi, J., Zhao, D., Wang, W.: 'Adaptive sliding mode fuzzy control for a two-dimensional overhead crane', Mechatronics, 2005, 15, (5), pp. 505–522

27 Sun, N., Fang, Y., Chen, H.: 'A new antiswing control method for underactuated cranes with unmodeled uncertainties: Theoretical design and hardware experiments', IEEE Transactions on Industrial Electronics, 2015, 62, (1), pp. 453–465

28 Tuan, L.A., Kim, J.J., Lee, S.G., Lim, T.G., Nho, L.C.: 'Second-order sliding mode control of a 3d overhead crane with uncertain system parameters', International Journal of Precision Engineering and Manufacturing, 2014, 15, (5), pp. 811–819

29 Xi, Z., Hesketh, T.: 'Discrete time integral sliding mode control for overhead crane with uncertainties', IET Control Theory and Applications, 2010, 4, (10), pp. 2071–2081

30 Lin, F.J., Shen, P.H.: 'Robust fuzzy neural network sliding-mode control for twoaxis motion control system', IEEE Transactions on Industrial Electronics, 2006, 53, (4), pp. 1209–1225

31 Wang, W., Yi, J., Zhao, D., Liu, D.: 'Design of a stable sliding-mode controller for a class of second-order underactuated systems', IET Proceedings - Control Theory and Applications, 2004, 151, (6), pp. 683–690

32 Close, C.M., Frederick, D.K.: 'Modeling and analysis of dynamic systems'. (Taylor & Francis, 2014)

33 Filippov, A.F.: 'Differential equations with discontinuous righthand sides', Journal of Mathematical Analysis & Applications, 1999, 154, (2), pp. 99–128

34 Nai, One, Lai, Christopher, Edwards, Sarah, et al.: 'Discrete output feedback sliding-mode control with integral action', International Journal of Robust & Nonlinear Control, 2006, 216, (1), pp. 21–43
35 Fang, Y., Ma, B., Wang, P., Zhang, X.: 'A motion planning-based adaptive control method for an underactuated crane system', IEEE Transactions on Control Systems Technology, 2011, 20, (1), pp. 241–248
36 Filippov, A.G.: 'Application of the theory of differential equations with discontinuous right-hand sides to non-linear problems in automatic control', IFAC Proceedings Volumes, 1960, 1, (1), pp. 933–937
37 Zheng, S.: 'Adaptive-impulsive function projective synchronization for a class of time-delay chaotic systems', Complexity, 2015, 21, (2), pp. 333–341

## 8 Appendix 1

### Variables in (12)

$$M_{11} = M_x + m \qquad M_{13} = ml\cos\theta_x\cos\theta_y$$
$$M_{14} = -ml\sin\theta_x\sin\theta_y \qquad M_{21} = 0$$
$$M_{22} = M_y + m \qquad M_{23} = 0$$
$$M_{24} = ml\cos\theta_y \qquad M_{31} = ml\cos\theta_x\cos\theta_y$$
$$M_{32} = 0 \qquad M_{33} = ml^2\cos^2\theta_y$$
$$M_{34} = 0 \qquad M_{41} = -ml\sin\theta_x\sin\theta_y$$
$$M_{42} = ml\cos\theta_y \qquad M_{43} = 0$$
$$M_{44} = ml^2$$

$$C_{13} = -ml\sin\theta_x\cos\theta_y\dot{\theta}_x - ml\cos\theta_x\sin\theta_y\dot{\theta}_y$$
$$C_{14} = -ml\cos\theta_x\sin\theta_y\dot{\theta}_x - ml\sin\theta_x\cos\theta_y\dot{\theta}_y$$
$$C_{23} = 0$$
$$C_{33} = -ml\sin\theta_y\dot{\theta}_y$$
$$C_{34} = -ml^2\sin\theta_y\cos\theta_y\dot{\theta}_x$$
$$C_{43} = ml^2\cos\theta_y\sin\theta_y\dot{\theta}_x$$
$$C_{44} = 0$$

## Appendix 2

### Variables in (37)

$$\begin{aligned}
\dot{V} =& S\dot{S}\\
=& S(I_1\dot{S}_1 + I_2\dot{S}_2)\\
=& S[I_1(\ddot{e}_p + H_1\dot{e}_p + \alpha(n/p)e_p^{n/p-1})\\
&+ I_2(\ddot{e}_\theta + H_2\dot{e}_\theta + \beta(n/p)e_\theta^{n/p-1})]\\
=& S[I_1(H_1\dot{e}_p + \alpha(n/p)e_p^{n/p-1} + (A_1(e) + B_1(e)U))\\
&+ I_2(H_2\dot{e}_\theta + \beta(n/p)e_\theta^{n/p-1} + (A_2(e) + B_2(e)U))]\\
=& S[I_1(H_1\dot{e}_p + \alpha(n/p)e_p^{n/p-1}\\
&+ (A_1(e) + B_1(e)(\sigma_1 + \sigma_2 + \sigma_{sw})))\\
&+ I_2(H_2\dot{e}_\theta + \beta(n/p)e_\theta^{n/p-1}\\
&+ (A_2(e) + B_2(e)(\sigma_1 + \sigma_2 + \sigma_{sw})))]\\
=& S[I_1\Pi_{11}(\sigma_2 + \sigma_{sw}) + I_2\Pi_{21}(\sigma_1 + \sigma_{sw})\\
&+ \alpha(n/p)e_p^{n/p-1} + \beta(n/p)e_\theta^{n/p-1}]\\
=& S[I_2\Pi_{21}\sigma_1 + I_1\Pi_{11}\sigma_2 + \alpha(n/p)e_p^{n/p-1}\\
&+ \beta(n/p)e_\theta^{n/p-1} + (I_1\Pi_{11} + I_2\Pi_{21})\sigma_{sw}].
\end{aligned}$$